Chinese Journal of Electronics
vol. 33, no. 2, pp. 463–471, March 2024
https://doi.org/10.23919/cje.2022.00.332

RESEARCH ARTICLE

A Wideband High-Gain Sawtooth Slot Array Antenna with Frequency-Scanning at Lower Frequency and Fixed-Beam at Higher Frequency

Qiang SUN, Yongling BAN, and Jun HU

School of Electronic Science and Engineering, University of Electronic Science and Technology of China, Chengdu 611730, China

Corresponding author: Yongling BAN, Email: byl@uestc.edu.cn
Manuscript Received September 30, 2022; Accepted March 21, 2023

Abstract — Exploring the multifunctional array antenna suitable for complex communication environment has very important research value. In this paper, a millimeter wave (mm-wave) double longitudinal sawtooth slot array antenna (DLSA) based on substrate integrated waveguide (SIW) technology is proposed, which has wideband, high-gain and novel beam characteristics. Two irregular longitudinal slots are etched on the SIW conductor surface as the radiation structure. To improve the bandwidth of the DLSA, the metallized vias are added at the transition point of the slots to construct multiple resonant frequency points. By adjusting the size of the slots and the position of the metallized vias, the phase constant can be regulated, and the unusual beam characteristics can be obtained. That is to say, in the lower frequency band, the beam pointing angle increases with frequency. In the higher frequency band, the beam pointing angle is maintained at a fixed angle. Finally, to improve the antenna gain, a 16 × 8 DLSA is fabricated, measured and discussed. The proposed antenna has an impedance matching bandwidth close to 9.7 GHz. From 27 to 33 GHz, the beam pointing angle changes from 8° to 29°. From 33 to 37 GHz, the beam pointing angle is fixed at 29°, and the pointing angle error range is ±1°. In addition, the measured maximum gain is 22.9 dBi at 32 GHz.

Keywords — Frequency-scanning, Fixed beam, High-gain, Millimeter-wave, Sawtooth slot, Wideband.
Citation — Qiang SUN, Yongling BAN, and Jun HU, "A Wideband High-Gain Sawtooth Slot Array Antenna with Frequency-Scanning at Lower Frequency and Fixed-Beam at Higher Frequency," *Chinese Journal of Electronics*, vol. 33, no. 2, pp. 463–471, 2024. doi: 10.23919/cje.2022.00.332.

I. Introduction

For the application of some special communication service environment, such as navigation, positioning and target monitoring, frequency-scanning antenna has the unique advantages of low cost, stability and reliability.

The beam pointing angle of the traditional frequency scanning antenna changes with the frequency [1]–[13] and the beam scanning can be realized without additional feeding network. It has the advantages of low loss and low design complexity. Notably, most communication systems realize wireless communication in a predetermined frequency band, and the beam pointing angle of the antenna needs to be fixed at an exact angle to achieve the point-to-point wireless communication [14]–[17]. However, the inherent dispersion of frequency-scanning antenna brings frequency-dependent beam scanning property, which is not applicable in conventional communication scenarios. To solve this problem, some scholars add active devices or dispersion compensation structure on the basis of the traditional frequency-scanning antenna, and adjust its effective phase constant to realize a fixed frequency beam-scanning array antenna [18]–[22] and fixed beam array antenna [23], [24]. However, the introduction of active devices will increase the loss of the antenna system, and the dispersion compensation structure will increase the size and complexity of the antenna.

With the emergence of a large number of wireless devices and wireless applications, the intertwined communication environment urgently requires the array antenna to have an integrated and versatile function. Un-

Associate Editor: Prof. Yongle WU, Beijing University of Posts and Telecommunications.

fortunately, most of the array antennas can only achieve a single beam characteristic of the fixed-beam or the frequency-scanning beam, there are fewer array antennas with two kinds of beam characteristics.

To deal with the complex communication environment, which needs two kinds of beam characteristics at the same time and relieve the pressure of limited space for loadable wireless communication equipment, a novel millimeter wave (mm-wave) double longitudinal sawtooth slot array antenna (DLSA) is presented in this paper. The proposed antenna can be applied to places where a variety of complex communication environments coexist, as shown in Figure 1. The proposed antenna has the feature of frequency-scanning in the lower frequency band, and can be used in traffic monitoring and communication of people and vehicles. In the higher frequency band, it can meet the wireless communication in some fixed equipment, e.g. autostereoscopic display on the roadside and large-scale display equipment. The advantage is that one antenna can be used in multiple communication environments, relieving the pressure of limited space for loadable wireless communication devices.

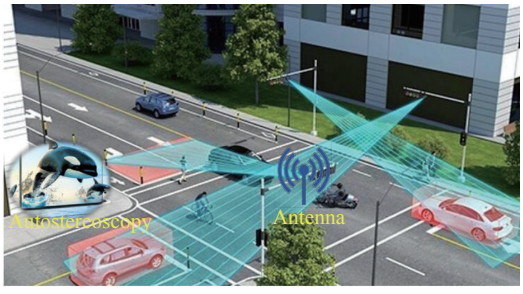

Figure 1 Communication environment of the proposed antenna.

The main contributions of this work are as follows:

1) The DLSA is proposed and analyzed.

2) This DLSA has a novel beam characteristic. That is, in the lower frequency band, the beam pointing angle changes linearly with the frequency; In the higher frequency band, the beam pointing angle hardly changes with frequency, pointing to a fixed angle.

The remainder of this paper is organized as follows. The principle and parameter analysis of the proposed array antenna are given in Section II. Section III presents the fabrication prototypes, measured and discussion results of the proposed antenna. And Section IV concludes this paper.

II. Antenna Design and Principle Analysis

Figure 2 illustrates the proposed 1 × 2 double longitudinal sawtooth slot array antenna. The radiation structure of the DLSA is constructed by etching two irregular longitudinal slots on the surface of substrate integrated waveguide (SIW) with thickness of 0.508 mm and the dielectric constant is 2.2. A metalized via is added at the transition line of the slot element to adjust the impedance matching of the antenna.

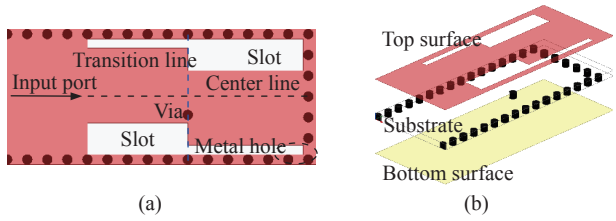

Figure 2 Geometry of the 1 × 2 DLSA. (a) Top view. (b) 3D view.

For the slot array antenna arranged along the x direction, as shown in Figure 3(a). Because the excitation currents of the two slot elements are reversed, which means that the phase difference between the slot elements is 180°, a dual-beam radiation pattern will be produced, as shown in Figure 3(b).

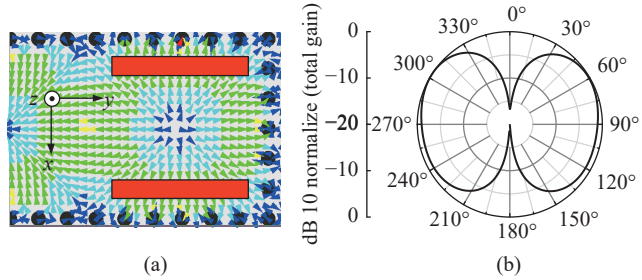

Figure 3 (a) Traditional double longitudinal slot array antenna. (b) E-plane radiation pattern.

In our work, by etching sawtooth slots on the surface of SIW and adding metallized vias in the transition line, the electric field mode and the surface current of cutting slot element can be changed. The electric field mode in SIW is changed from cylindrical distribution to sawtooth distribution, as shown in Figure 4(a).

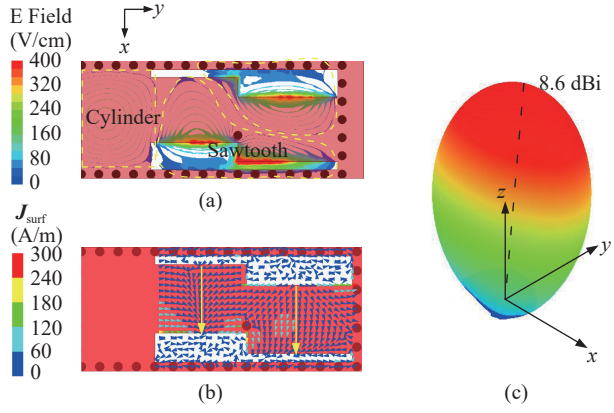

Figure 4 1 × 2 DLSA (a) Electric field amplitude distribution at 30 GHz. (b) Surface current distribution. (c) Radiation pattern.

The desired current distribution can be generated, as shown in Figure 4(b). Such a current distribution can ensure that the slot elements along the x direction have the same phase current excitation. The adjacent current along the y direction is also in the same direction, but there is a small angle phase difference, which makes the beam tilt along the broadside direction. That is to say, the 1 × 2 DLSA can produce a single beam, the cross

section radiation pattern along the x direction will not produce dual-beam phenomenon. Because there is a little excitation phase difference between the adjacent elements along the y direction, the cross section radiation pattern along the y direction will produce a single beam deviating from the broadside direction, as illustrated in Figure 4(c).

1. Wideband characteristics

Figure 5 shows three different sizes of the DLSAs, namely the 1 × 2 DLSA, the 1 × 4 DLSA and the 1 × 8 DLSA. Notably, the SIW width of the three DLSAs is a_0, the length of the first metal patch and the last metal patch of the three DLSAs are a_{14} and a_5, respectively, and the length of all the remaining patches are a_{19}. The detailed parameters of the three different sizes of DLSAs are listed in Table 1.

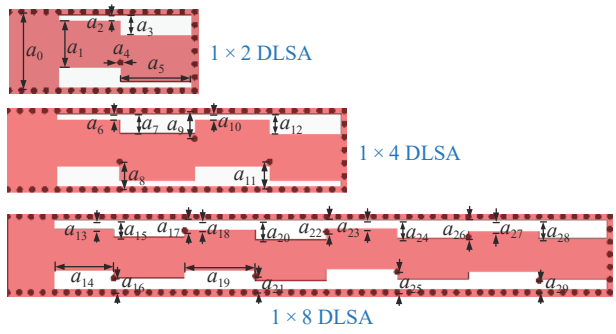

Figure 5 Different sizes of the DLSAs.

Table 1 Dimensions of the antennas (Unit: mm)

Parameters	a_0	a_1	a_2	a_3	a_4	a_5	a_6	a_7
Value	5.00	2.94	0.35	1.25	0.40	4.60	0.35	1.25
Parameters	a_8	a_9	a_{10}	a_{11}	a_{12}	a_{13}	a_{14}	a_{15}
Value	1.78	1.78	0.36	1.78	1.26	0.65	4.00	1.14
Parameters	a_{16}	a_{17}	a_{18}	a_{19}	a_{20}	a_{21}	a_{22}	a_{23}
Value	0.92	0.92	0.67	4.8	1.33	1.07	1.01	0.57
Parameters	a_{24}	a_{25}	a_{26}	a_{27}	a_{28}	a_{29}	–	–
Value	1.23	1.36	1.36	0.76	1.26	0.78	–	–

Figure 6 shows the reflection coefficients for four different sizes of the DLSAs, and their impedance matching bandwidth ($S_{11} < -10$ dB) are 22.7% @30 GHz, 27.5% @30 GHz, 44.8% @30 GHz and 45.2% @30 GHz, respectively. As the size of the array antenna increases, the impedance matching bandwidth is also increasing. It is worth noting that the bandwidth of the 1 × 16 DLSA is not significantly improved compared to the 1 × 8 DLSA. Their impedance matching bandwidth is controlled by the adjustment capabilities of the slots and metallized vias.

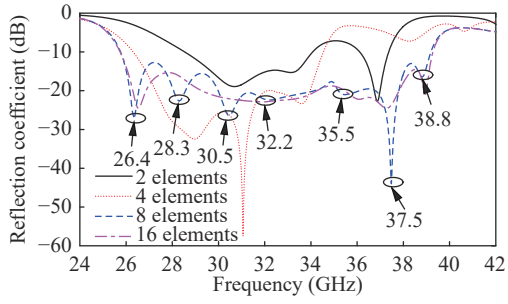

Figure 6 Reflection coefficients for different elements of the DLSAs.

2. Beam characteristics

Figure 7 shows the H-plane radiation patterns of the 1 × 8 DLSA. The minimum gain is 12.7 dBi at 34 GHz, and the maximum gain is 14.9 dBi at 37 GHz. It is worth noting that from 26 to 33 GHz, the beam pointing angle increases with frequency and the beam pointing angles are 4°, 8°, 13°, 17°, 21°, 24°, 27°, and 29°, respectively. However, from 33 to 38 GHz, the beam pointing angle is a fixed angle 29°, and the beam pointing angle error range is ±1°. The pointing angle, gain, sidelobe level and radiation efficiency of the 1 × 8 DLSA are listed in Table 2.

Figure 8 shows the approximate equivalent circuit of the 1 × 8 DLSA. The top and the bottom conductors of the SIW are equivalent to two transmission lines with series inductance L_{T1} and the shunt capacitance C_T. The two rows of metallized vias are equivalent to the shunt inductance L_{T2}. The metalized vias at the transition line are equivalent to the shunt inductance L_{Vi} $(i = 1, 2, \ldots, 7)$. The metal patches between the slots are equivalent to the series inductance L_{Pi} $(i = 1, 2, \ldots, 8)$. The slot element is equivalent to the shunt capacitance C_i $(i = 1, 2, \ldots, 8)$. R is radiation resistance.

According to [25], the phase constant can be obtained by the impedance Z of the series stub and the admittance Y of the shunt stub.

$$\gamma = \alpha + \mathrm{j}\beta = \sqrt{ZY} \tag{1}$$

When the loss α is not considered, the phase constant can be determined by the capacitance and inductance, as shown in (2).

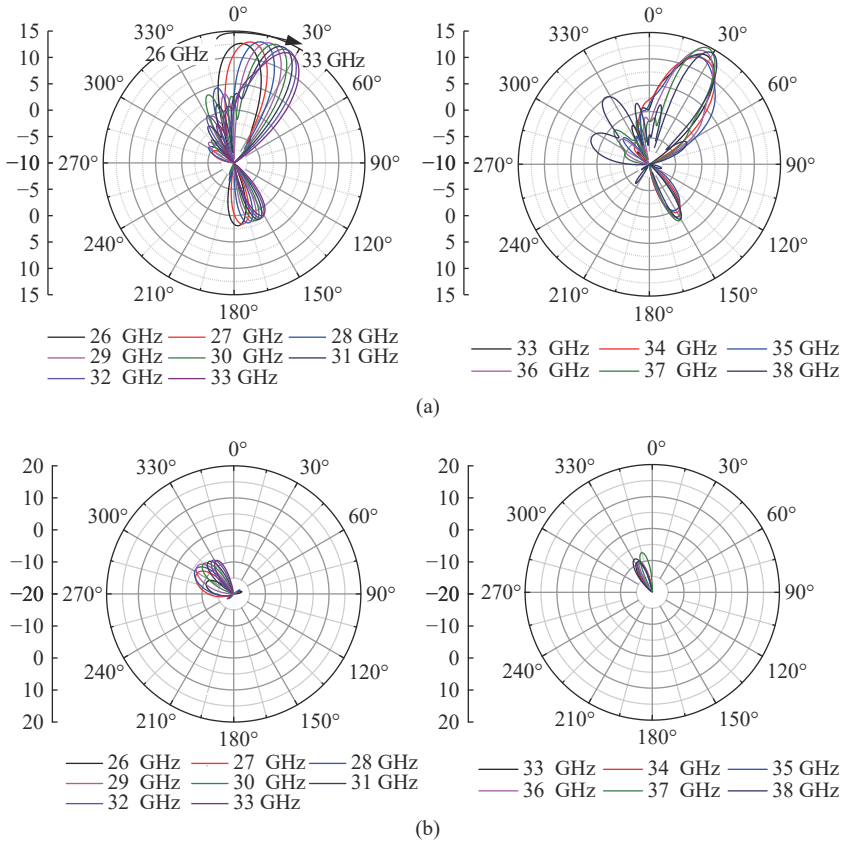

Figure 7 H-plane radiation patterns of the 1 × 8 DLSA. (a) Main polarization. (b) Cross-polarization.

Table 2 Performance of the 1 × 8 DLSA

Frequency (GHz)	26	28	30	32	34	36	38
Pointing angle (°)	4	13	21	27	29	28	30
Gain (dB)	12.72	13.54	13.85	13.73	12.62	13.87	14.66
Sidelobe level (dB)	−18.4	−9.0	−10.5	−14.4	−17.3	−16.0	−9.2
Radiation efficiency (%)	97.2	98.0	98.5	99.0	99.2	98.9	96.0

$$\beta = \sqrt{\left(\mathrm{j}\omega L_{\mathrm{T}} + \frac{1}{\mathrm{j}\omega C_8}\right)\left(\mathrm{j}\omega C_{\mathrm{T}} + \frac{1}{\mathrm{j}\omega L_{\mathrm{C}}}\right)} \tag{2}$$

where $\frac{1}{L_{\mathrm{C}}}=\frac{1}{L_{T2}}+\frac{1}{L_{v1}}+\frac{1}{L_{v2}}+\frac{1}{L_{v3}}+\frac{1}{L_{v4}}+\frac{1}{L_{v5}}+\frac{1}{L_{v6}}+\frac{1}{L_{v7}}$, $L_{\mathrm{T}}=L_{\mathrm{T1}}+L_{\mathrm{P1}}+L_{\mathrm{P2}}+L_{\mathrm{P3}}+L_{\mathrm{P4}}+L_{\mathrm{P5}}+L_{\mathrm{P6}}+L_{\mathrm{P7}}+L_{\mathrm{P8}}$, $C_{\mathrm{T}}=CT+C_1+C_2+C_3+C_4+C_5+C_6+C_7+C_8$.

Because the proposed DLSA is a single-port non-periodic structure, and the phase constant curve cannot be obtained by *S*-parameters. The relationship curve between the beam pointing angle θ and the frequency can be obtained by fitting the sampling points, which is shown in Figure 9(a). The relationship curve between phase constant β and frequency can be calculated by (3), which is drawn in Figure 9(b). In addition, the calculated phase constant curve are given in Figure 9(b).

$$\theta = \arcsin\left(\beta/k_0\right) \tag{3}$$

where k_0 is the free space wave number.

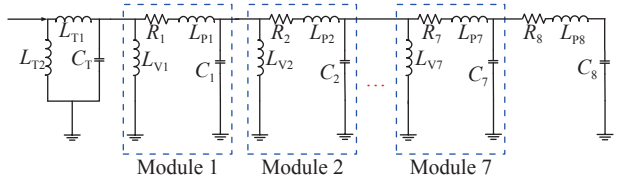

Figure 8 Approximate equivalent circuit of the 1 × 8 DLSA.

From 24 to 33 GHz, the relationship curve between phase constant and frequency is approximately linear. From 33 to 38 GHz, the phase constant basically does not change with frequency, showing a flat distribution. The impedance Z and admittance can be regulated by the sawtooth slots and the metallized vias. Therefore, by adjusting the slots width and the position of the metalized vias to make the phase constant equation meet the curve shown in Figure 9(b), the DLSA with frequency-scanning characteristics in the lower frequency band and fixed-beam characteristics in the higher frequency band can be realized.

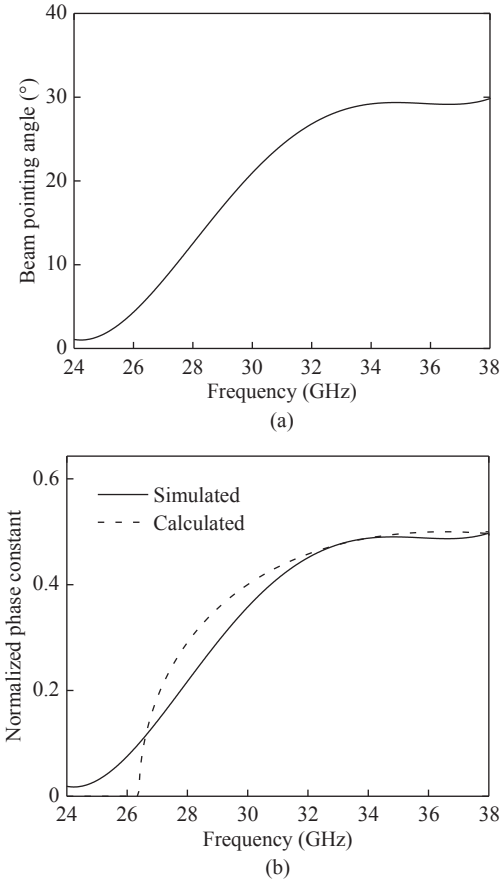

Figure 9 (a) Beam pointing angle and (b) Normalized phase constants of the 1 × 8 DLSA ($L_T = 5$ nH, $C_8 = 2.1$ nF, $C_T = 8$ nF, and $L_C = 4.55$ nH).

3. Parameters analysis

The proposed 1 × 8 DLSA has a non-periodic structure and involves many parameters. To facilitate the analysis of different types of parameters on the phase constant, the same type of parameters are set as the same size. Finally, there are four parameters can be analyzed. The distance between the center of the metal patch and the center line of SIW is offset, the distance between the metalized vias and the SIW boundary is x_1, the length of the slot element is l, and the width of the metal patch is w, as shown in Figure 10. The beam pointing angle and the phase constant have a consistent relationship. Therefore, the beam pointing angle curve can be used to characterize the phase constant curve.

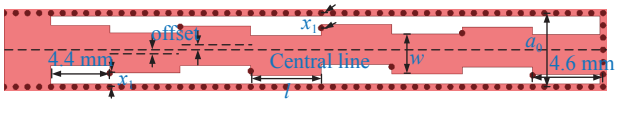

Figure 10 1 × 8 DLSA.

The *S*-parameters and phase constant curves with different parameters are drawn in Figure 11. The parameters offset and x_1 have little effect on the frequency migration, but they will affect the resonance frequency points. The *offset* parameter has a great influence on the phase constant curve in the higher frequency. When the value of the x_1 parameter decreases, the frequency-scanning characteristic can be realized in the entire frequency band, as shown in Figure 11(d).

The width and length of the metal patch have a greater impact on the impedance matching. When the width w and the length l of the metal patch are changed, the phenomenon of frequency band migration will occur. When the width of the metal patch is reduced, the entire frequency band will migration to high frequencies. When the length of the metal patch is increased, the shape of the resonance frequency point changes little, and the entire frequency band migration to the low frequency band, as shown in Figures 11(e) and (g). The length and width of the metal patch have different effects on the phase constant curves. When the width of the metal patch is changed, the phase constant curve changes more drastically in the high frequency range. That is, when the width of the metal patch decreases, the phase constant gradually becomes flat in the higher frequency band. The increase in the length of the metal patch will make the phase constant curve move up as a whole.

Therefore, by adjusting the size of the DLSA, under the premise of ensuring the good impedance matching bandwidth, the beam characteristics of frequency-scanning in the lower frequency band and the fixed beam in the higher frequency band can be achieved. Finally, the limitation of the downlink cutoff frequency of the proposed 1 × 8 DLSA is briefly described. The SIW width of our initial design is 5 mm, because the voltage standing wave ratio under this width is the smallest at 30 GHz, its cutoff frequency is 23.71 GHz. Therefore, the cutoff frequency of the 1 × 8 DLSA can be shifted by changing the width of the SIW.

III. Fabrication, Measurement and Discussion

The proposed array antenna are obtained by ANSYS HFSS V19.0. The substrate is Rogers RT/duroid 5880 with dielectric constant of 2.2, the loss tangent is 0.0009 and the thickness is 0.508 mm. The scattering coefficients and radiation patterns are measured by the Agilent E8363B network analyzer and the millimeter wave (mm-wave) anechoic chamber, respectively.

1. *S*-parameters

To achieve a high gain array antenna, Figure 12 shows the simulation and fabrication models of the single-port excited 16 × 8 DLSA. A power division network of 1 to 16 is used to obtain the high gain array antenna. Figure 13 shows the simulated and measured reflection coefficients. The solid and dashed line represent the measured and simulated results, respectively. In the range of 26 to 38 GHz, the simulated and measured impedance matching bandwidths ($S_{11} < -10$ dB) are 9.34 and 9.66 GHz, respectively.

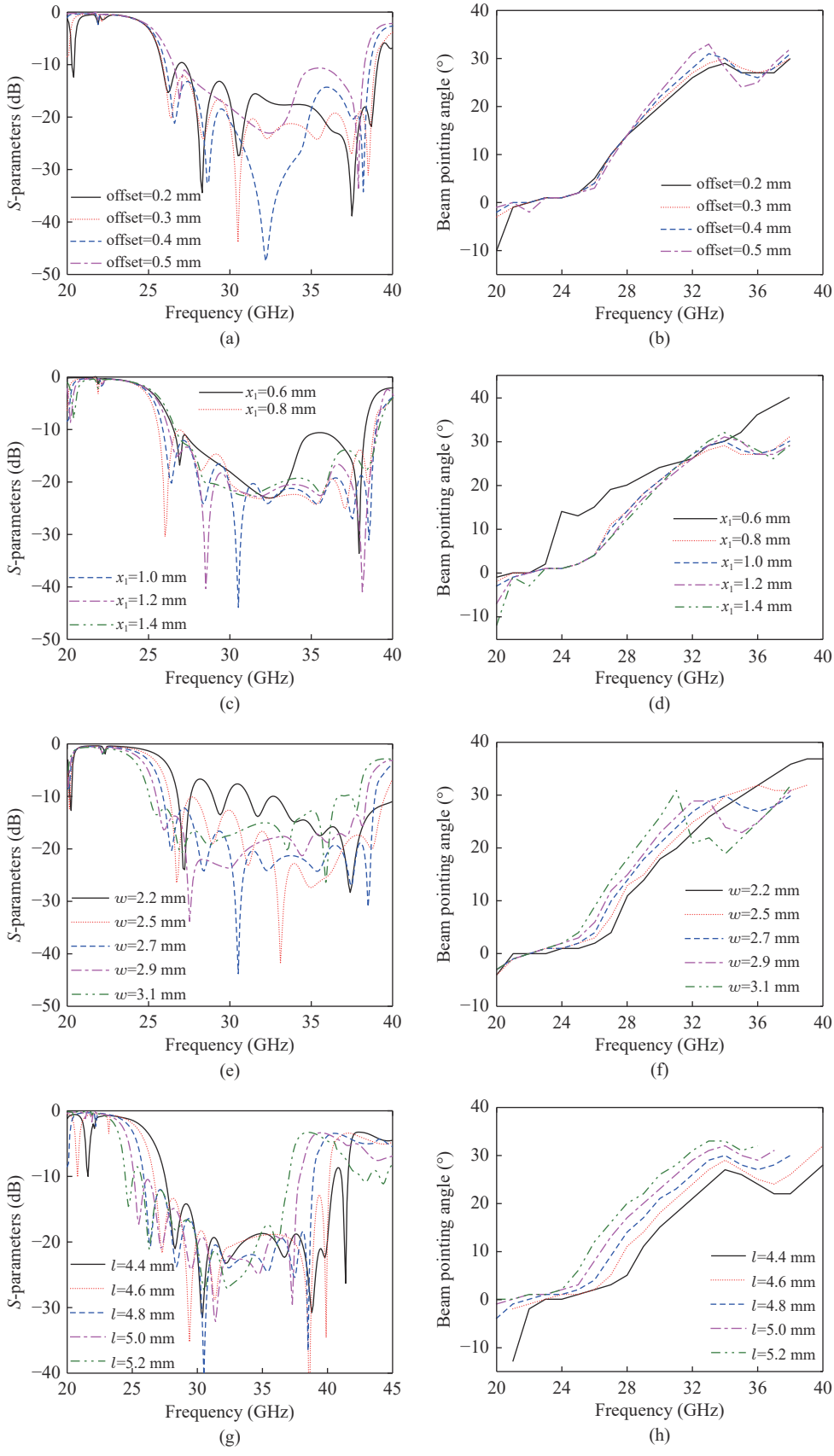

Figure 11 (a) S-parameters with different offset. (b) Beam pointing angle with different offset. (c) S parameters with different x_1. (d) Beam pointing angle with different x_1. (e) S parameters with different w. (f) Beam pointing angle with different w. (g) S parameters with different l. (h) Beam pointing angle with different l.

Figure 12 Proposed 16 × 8 DLSA. (a) Simulation model. (b) Photographs of the fabricated array antenna.

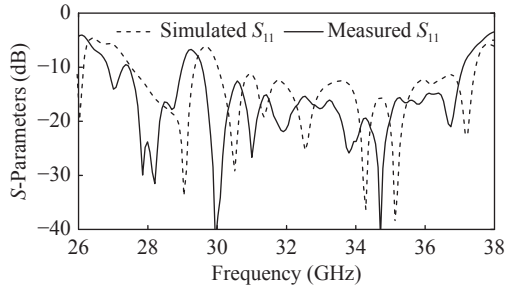

Figure 13 Simulation and measurement of the reflection coefficient.

2. Radiation patterns and gains

Figure 14 shows the measured and simulated normalized radiation patterns. Similarly, the solid and dashed lines represent measured and simulated results, respectively. From 27 to 33 GHz, the measured beam pointing angles are 8°, 13°, 17°, 21°, 24°, 27°, and 29°, respectively. From 33 to 37 GHz, the measured beam pointing angles are 29°, and the beam pointing angle error range is ±1°.

To evaluate the radiation performance of the 16 × 8 DLSA. Figure 15 shows the simulated and measured gain curves. In the range of 27 to 37 GHz, the simulated and measured gain ranges of the 16 × 8 DLSA are 21.89 to 24.5 dBi and 20.79 to 22.9 dBi, respectively.

3. Comparison and discussion

To make a distinction and comparison, the comparisons between the proposed DLSA and the traditional slot array antenna are listed in Table 3. Compared with the traditional slot array antenna with frequency-scanning [2]–[9], the proposed antenna has not only the beam characteristics of frequency-scanning, but also has fixed-beam characteristics. Compared with the traditional fixed-beam slot array antenna [26], [27], the proposed array antenna has the characteristics of frequency-scanning. In addition, the proposed antenna has the advantages of high gain and wideband.

IV. Conclusion

In this paper, a novel mm-wave DLSA is constructed by etching two irregular longitudinal slots on the SIW conductor edge and adding metallized vias in the SIW. By adjusting the slot elements and metallized vias, the original electromagnetic field mode in SIW can be changed, and the unusual radiation characteristics can be obtained. That is to say, the beam scanning angle changes with the frequency from 27 to 33 GHz, and the beam pointing angle is fixed at a specific angle from 33 to 37 GHz. In a word, the proposed DLSA with wideband and high gain can be used as an alternative candidate for integrated multipurpose mm-wave array antenna in the complex communication environment.

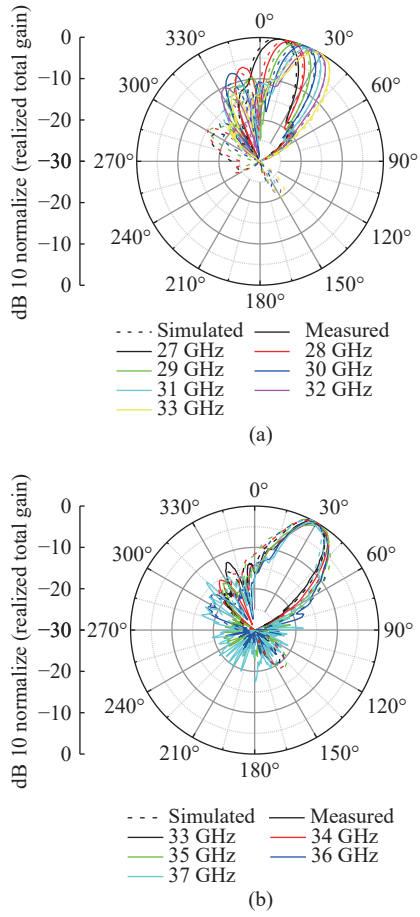

Figure 14 Measured and simulated normalized radiation patterns. (a) 27-33 GHz. (b) 33-37 GHz.

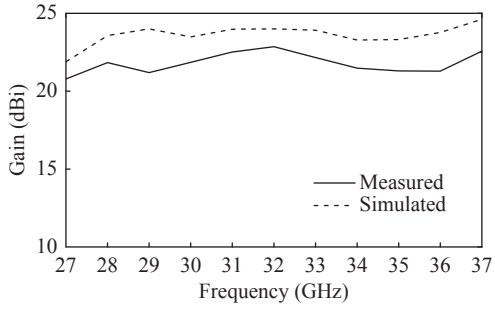

Figure 15 Simulated and measured gains of the 16×8 DLSA.

Acknowledgement

This work was supported by the National Natural Science Foundation of China (Grant Nos. 61971098 and U19A2055), the National Key Research and Development

Table 3 Comparison between traditional slot array antenna and the proposed DLSA

Ref.	Transmission line	Number of elements	Bandwidth (GHz)	Beam type	Peak gain (dBi)	Scanning angle
[2]	SIW	1 × 19	10–17.5 (54.5%)	Frequency-scanning	14.2	−49° to +69°
[3]	RSIW	1 × 8	8–12 (40%)	Frequency-scanning	12.5	−35° to +35°
[4]	SIW	1 × 14	8.5–14.4 (51.5%)	Frequency-scanning	15	−53° to +37°
[5]	SIW	1 × 21	16.5–23.1 (33.3%)	Frequency-scanning	19.8	−90° to −10°
[6]	CRLH SIW	1 × 11	16.5–23.01 (33.3%)	Frequency-scanning	18	248°
[7]	SIW	N.A.	10–12.8 (24.6%)	Frequency-scanning	16.8	+31.4° to +50.5°
[8]	SIW	1 × 15	16–18 (11.8%)	Frequency-scanning	>9.1	−56° to +48°
[9]	SIW	1 × 19	10.5–17.5 (50%)	Frequency-scanning	16.5	−64° to +20°
[26]	SIW	1 × 4	5.4–6.45 (17.7%)	Fixed-beam	8	0°
[27]	RSIW	4 × 4	25.45–27.75 (8.6%)	Fixed-beam	14.5	0°
Proposed	SIW	16 × 8	27–37 (31.3%)	Frequency-scanning and fixed-beam	22.9	8° to 29°, 29°

Project (Grant No. 2020YFB1805003), and the Fund of Science and Technology on Electromagnetic Scattering Laboratory (Grant No. 61424090410).

References

[1] K. M. Mak, K. K. So, H. W. Lai, *et al.*, "A magnetoelectric dipole leaky-wave antenna for millimeter-wave application," *IEEE Transactions on Antennas and Propagation*, vol. 65, no. 12, pp. 6395–6402, 2017.

[2] R. Ranjan and J. Ghosh, "SIW-based leaky-wave antenna supporting wide range of beam scanning through broadside," *IEEE Antennas and Wireless Propagation Letters*, vol. 18, no. 4, pp. 606–610, 2019.

[3] A. Mallahzadeh and S. Mohammad-Ali-Nezhad, "Periodic collinear-slotted leaky wave antenna with open stopband elimination," *IEEE Transactions on Antennas and Propagation*, vol. 63, no. 12, pp. 5512–5521, 2015.

[4] D. K. Karmokar, S. L. Chen, D. Thalakotuna, *et al.*, "Continuous backward-to-forward scanning 1-D slot-array leaky-wave antenna with improved gain," *IEEE Antennas and Wireless Propagation Letters*, vol. 19, no. 1, pp. 89–93, 2020.

[5] M. Z. Ali and Q. U. Khan, "High gain backward scanning substrate integrated waveguide leaky wave antenna," *IEEE Transactions on Antennas and Propagation*, vol. 69, no. 1, pp. 562–565, 2021.

[6] A. Sarkar, A. Sharma, A. Biswas, *et al.*, "Compact CRLH leaky-wave antenna using TE_{20}-mode substrate-integrated waveguide for broad space radiation coverage," *IEEE Transactions on Antennas and Propagation*, vol. 68, no. 10, pp. 7202–7207, 2020.

[7] A. M. Malekshah, M. S. Majedi, and A. R. Attari, "Improved design of uniform SIW leaky wave antenna with suppression of unwanted mode," *IEEE Access*, vol. 9, pp. 157623–157627, 2021.

[8] K. W. Xu, Q. Wang, L. H. Lv, *et al.*, "SIW-based -band leaky-wave antenna with improved beam steering performance," *IEEE Antennas and Wireless Propagation Letters*, vol. 21, no. 11, pp. 2224–2228, 2022.

[9] R. Ranjan and J. Ghosh, "Substrate integrated waveguide leaky wave antenna using longitudinal slots for seamless wide angle scanning with enhanced gain," *International Journal of RF and Microwave Computer-Aided Engineering*, vol. 31, no. 9, article no. e22770, 2021.

[10] W. Jiang, C. J. Liu, B. Zhang, *et al.*, "K-band frequency-scanned leaky-wave antenna based on composite right/left-handed transmission lines," *IEEE Antennas and Wireless Propagation Letters*, vol. 12, pp. 1133–1136, 2013.

[11] Y. L. Chiou, J. W. Wu, J. H. Huang, *et al.*, "Design of short microstrip leaky-wave antenna with suppressed back lobe and increased frequency scanning region," *IEEE Transactions on Antennas and Propagation*, vol. 57, no. 10, pp. 3329–3333, 2009.

[12] X. M. Lv, W. Q. Cao, Z. Y. Zeng, *et al.*, "A circularly polarized frequency beam-scanning antenna fed by a microstrip spoof SPP transmission line," *IEEE Antennas and Wireless Propagation Letters*, vol. 17, no. 7, pp. 1329–1333, 2018.

[13] D. S. Liao, Y. F. Zhang, and H. G. Wang, "Wide-angle frequency-controlled beam-scanning antenna fed by standing wave based on the cutoff characteristics of spoof surface Plasmon polaritons," *IEEE Antennas and Wireless Propagation Letters*, vol. 17, no. 7, pp. 1238–1241, 2018.

[14] Z. Ahmed, M. John, P. Mcevoy, *et al.*, "Investigation of frequency scanning printed Bruce array antenna," *IEEE Access*, vol. 8, pp. 189003–189012, 2020.

[15] F. K. Sharifabad, M. A. Jensen, and A. L. Anderson, "Array beamforming synthesis for point-to-point MIMO communication," *IEEE Transactions on Antennas and Propagation*, vol. 63, no. 9, pp. 3878–3886, 2015.

[16] M. A. Almoteriy, M. I. Sobhy, and J. C. Batchelor, "Characterization of wideband antennas for point-to-point communications," *IEEE Transactions on Antennas and Propagation*, vol. 66, no. 9, pp. 4466–4473, 2018.

[17] V. Jaeck, L. Bernard, K. Mahdjoubi, *et al.*, "A conical patch antenna array for agile point-to-point communications in the 5.2-GHz band," *IEEE Antennas and Wireless Propagation Letters*, vol. 15, pp. 1230–1233, 2016.

[18] T. Lou, X. X. Yang, H. T. Qiu, *et al.*, "Low-cost electrical beam-scanning leaky-wave antenna based on bent corrugated substrate integrated waveguide," *IEEE Antennas and Wireless Propagation Letters*, vol. 18, no. 2, pp. 353–357, 2019.

[19] A. Suntives and S. V. Hum, "A fixed-frequency beam-steerable half-mode substrate integrated waveguide leaky-wave antenna," *IEEE Transactions on Antennas and Propagation*, vol. 60, no. 5, pp. 2540–2544, 2012.

[20] J. W. Lian, H. Zhu, Y. L. Ban, *et al.*, "Uniplanar high-gain 2-D scanning leaky-wave multibeam array antenna at fixed frequency," *IEEE Transactions on Antennas and Propagation*, vol. 68, no. 7, pp. 5257–5268, 2020.

[21] D. K. Karmokar, K. P. Esselle, and S. G. Hay, "Fixed-frequency beam steering of microstrip leaky-wave antennas using binary switches," *IEEE Transactions on Antennas and Propagation*, vol. 64, no. 6, pp. 2146–2154, 2016.

[22] L. Chang, Y. Li, Z. J. Zhang, *et al.*, "Reconfigurable 2-bit fixed-frequency beam steering array based on microstrip line," *IEEE Transactions on Antennas and Propagation*, vol. 66, no. 2, pp. 683–691, 2018.

[23] R. T. Hong, J. Q. Shi, D. F. Guan, *et al.*, "Air-filled sub-

strate integrated waveguide leaky-wave antenna with wideband and fixed-beam characteristics," *IEEE Transactions on Antennas and Propagation*, vol. 68, no. 10, pp. 7184–7189, 2020.

[24] J. F. Chen, W. Yuan, C. Zhang, *et al.*, "Wideband leaky-wave antennas loaded with gradient metasurface for fixed-beam radiations with customized tilting angles," *IEEE Transactions on Antennas and Propagation*, vol. 68, no. 1, pp. 161–170, 2020.

[25] C. Caloz and T. Itoh, *Electromagnetic Metamaterials*: *Transmission Line Theory and Microwave Applications*. John Wiley & Sons, Hoboken, NJ, USA, pp.59–79, 2005.

[26] Y. Q. Wen, B. Z. Wang, and X. Ding, "Wide-beam SIW-slot antenna for wide-angle scanning phased array," *IEEE Antennas and Wireless Propagation Letters*, vol. 15, pp. 1638–1641, 2016.

[27] Y. Ding and K. Wu, "A 4 × 4 ridge substrate integrated waveguide (RSIW) slot array antenna," *IEEE Antennas and Wireless Propagation Letters*, vol. 8, pp. 561–564, 2009.

Qiang SUN graduated from the North China University of Water Resources and Electric Power in 2017. He is currently pursuing the Ph.D. degree in electromagnetic field and microwave technology with the University of Electronic Science and Technology of China, Chengdu, China. His current research interests include millimeter wave antennas and arrays. (Email: sunqiang@std.uestc.edu.cn)

Yongling BAN received the B.S. degree in mathematics from Shandong University, the M.S. degree in electromagnetics from Peking University, and the Ph.D. degree in microwave engineering from the University of Electronic Science and Technology of China (UESTC), in 2000, 2003, and 2006, respectively. In July of 2006, he joined the Xi'an Mechanical and Electric Information Institute as a microwave engineer. He then joined Huawei Technologies Co., Ltd., Shenzhen, China. At Huawei, he designed and implemented various terminal antennas for 15 data card and mobile phone products customized from leading telecommunication industries like Vodafone. From September 2010 to July 2016, he was an Associate Professor with UESTC and is currently Professor with UESTC. From May 2014 to April 2015, he visited Queen Mary University of London as a Scholar Visitor. His research interests include wideband antennas for 5G devices, MIMO antenna, and millimeter wave antenna array. He is the author of over 130 referred journal and conference papers on these topics. Prof. Ban holds 20 granted and pending chinese and overseas patents. (Email: byl@uestc.edu.cn)

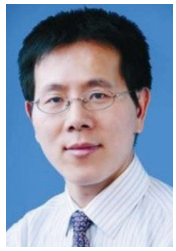

Jun HU received the B.S., M.S., and Ph.D. degrees in electromagnetic field and microwave technique from the University of Electronic Science and Technology of China (UESTC), Chengdu, China, in 1995, 1998, and 2000, respectively. In 2001, he was with the Center of Wireless Communication, City University of Hong Kong, Hong Kong, as a Research Assistant. From March to August 2010, he was a Visiting Scholar with the Electro Science Laboratory, Department of Electrical and Computer Engineering, The Ohio State University. He was a Visiting Professor with the City University of Hong Kong from February to March 2011. He is currently a Full Professor with the School of Electronic Science and Engineering, UESTC. Since September 2017, he has been the Vice President of UESTC. He is the author or the coauthor of over 300 technical articles. His current research interests include integral equation methods in computational electromagnetics, electromagnetic scattering, and radiation. Dr. Hu received the 2004 Best Young Scholar Paper Prize of the Chinese Radio Propagation Society, the 2014 National Excellent Youth Fund by the NSFC, the Chang Jing Scholar in 2016, and many best student papers awards. He was a co-recipient of the 2018 IEEE AP-S Sergei A. Schelkunoff Transaction Paper Award. He also served as the Chairman for the Student Activities Committee, IEEE Chengdu Section, from 2010 to 2016, and the IEEE Chengdu AP/EMC Joint Chapter from 2014 to 2016. (Email: hujun@uestc.edu.cn)